Appl Phys B (2010) 100: 265–273
DOI 10.1007/s00340-010-3993-y

Applied Physics B
Lasers and Optics

Pulsed quantum-cascade-laser spectroscopy with intermediate-size pulses: application to NH_3 in the 10 µm region

B. Grouiez · V. Zeninari · L. Joly · B. Parvitte

Received: 10 September 2009 / Revised version: 4 March 2010 / Published online: 27 March 2010
© Springer-Verlag 2010

Abstract Pulsed quantum-cascade-laser spectrometers are usually used to detect atmospheric gases with either the interpulse technique (short pulses, typically 5–20 ns) or the intrapulse technique (long pulses, typically 500–800 ns). Each of these techniques has its drawbacks. Particularly the gas absorption spectra are generally distorted. We have previously developed another technique called intermediate-size pulses (typically 50–100 ns) technique for gas detection using pulsed QCL spectrometers. In this paper, infrared spectra of ammonia recorded with this technique in the 10 µm region are presented. For the NH_3 spectra recorded at low pressure (i.e. in the mbar range), the spectra show typical oscillations after the absorption. The Beer–Lambert law cannot explain these oscillations, termed the rapid-passage effect. Comparisons between experimental and calculated spectra will be realized. This phenomenon is not satisfactory from a spectroscopic point of view and spectra must be recorded at higher pressures. For the NH_3 spectra recorded at higher pressure (i.e. in the 50 mbar range), the oscillations disappear and the Beer–Lambert law could be reused. This paper will demonstrate that the intermediate-size technique gives reliable measurements for NH_3 detection. Moreover the typical apparatus function (0.003 cm^{-1} HWHM) is far lower from the typical apparatus function of the interpulse QCL spectrometers (0.015 cm^{-1} HWHM).

B. Grouiez · V. Zeninari (✉) · L. Joly · B. Parvitte
Groupe de Spectrométrie Moléculaire et Atmosphérique, UMR CNRS 6089, Université de Reims Champagne-Ardenne, UFR Sciences Exactes et Naturelles, Moulin de la Housse, BP 1039, 51687 Reims Cedex 2, France
e-mail: virginie.zeninari@univ-reims.fr
Fax: +33-03-26913147

Present address:
B. Grouiez
CEA Saclay, 91190 Gif-sur-Yvette cedex, France

1 Intermediate-size pulse quantum-cascade-laser spectrometry

Quantum-cascade lasers (QCLs) are ideal mid-IR sources for trace gas monitoring. They can be fabricated to operate at any of a very wide range of wavelengths from 3 to 30 µm where the absorption gas coefficients are stronger than in the near-infrared. Various techniques using continuous wave (cw) QCLs have been tested in the Reims laser group demonstrating very beautiful results from a spectroscopic point of view [1–8]. A comparison between the cw and the pulsed modes for a quantum-cascade laser has been realized in [9]. Despite the good results obtained with cw devices, pulsed mode operation has long been the main way for using QCLs [10] and remains the only available technique for several spectral ranges [11]. Two different ways of pulsing the laser have been demonstrated.

The first way is used by most spectrometers based on pulsed QCLs [12, 13] and is based on a short-duration current pulse applied to the QCL. This current generates a pulse in the spectral domain, which can be tuned through the absorption feature of interest by use of a slowly varying subthreshold current ramp or by use of a variation of the temperature of the laser chip but at much lower speed, owing to the high thermal capacity of the laser submount and laser base. The main drawback associated with this method is related to the laser line broadening that reduces spectral resolution and sensibility. The "line broadening" that is often attributed to the laser line width is in fact related to the detector's bandwidth [14].

The other method for pulsing QCL differs from the previous one. It uses the linear frequency downchirp that is induced when a long top-hat current pulse is applied to a QCL. The temporal profile of a generated pulse is recorded and used to infer the spectral nature of the pulse. The extent of the frequency window that is covered depends on the

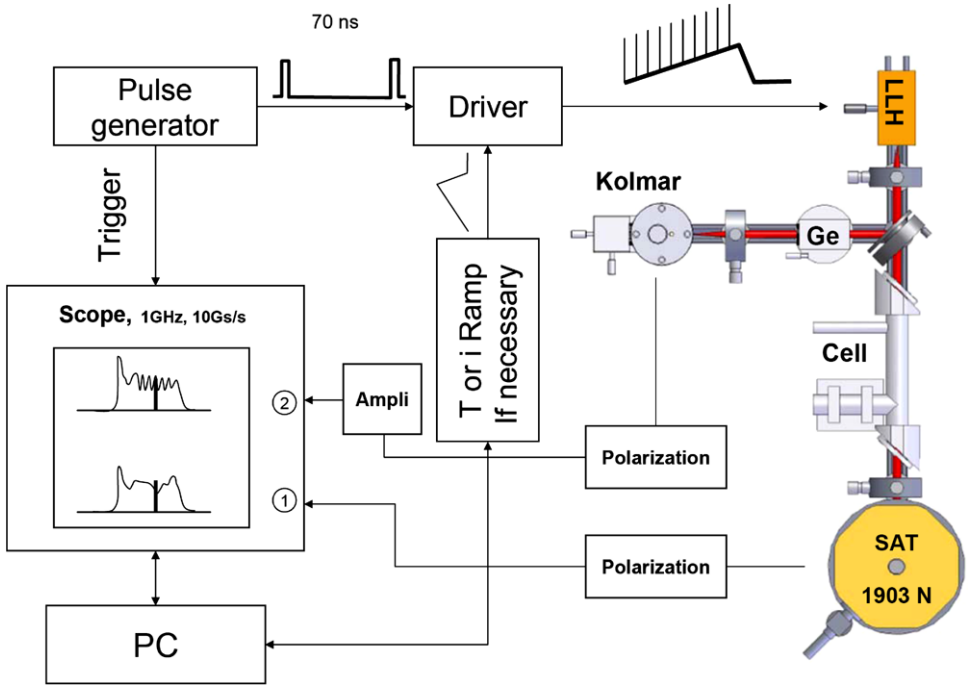

Fig. 1 Schematics of the experimental set-up

duration of the applied current pulse [15]. The spectral profiles of molecular gases can be recorded in real time [9, 16]. With this "long pulse" method, the resolution of the QCL spectrometer is limited not by the effective line width but by the temporal resolution of the detection system. Under some experimental conditions (low-pressure spectra, for example) the correlation between temporal and spectral profiles is not necessary straightforward. Particularly, if the duration of the interaction between the laser pulse and the molecular gas is short in comparison with the collisional lifetime, saturation and rapid-passage effects can occur as demonstrated in [17, 18].

Although this technique has numerous advantages when compared to the short-pulse technique, it suffers from several drawbacks: it requires much more specific instrumentation than the short-pulse technique, such as high-speed detectors and preamplifiers, a high-speed acquisition board, or a digital sampling oscilloscope. Moreover, the use of such long pulses is not recommended for most of the currently commercially available pulsed QCLs provided by Alpes Lasers [19]. Lasers allowing the use of long pulses seem to be available only for fewer wavelengths.

As none of those methods was completely satisfactory, a third way has been developed that uses intermediate length pulses, typically between 30 and 80 ns [14]. This interval of pulse duration was chosen to reach the linear frequency variation area that follows the transient at the beginning of the pulse without damaging the QC laser. We expected to obtain a narrower line width than with short pulses. The spectral range that is scanned inside so short pulses is usually small and we use either a subthreshold ramp (duty cycle of 0.3% with a frequency of 100 Hz) or a substrate temperature variation (duty cycle of 1% and ramping rate of 0.06 cm^{-1}/min) to increase the spectral range. These experiments were performed with a setup described in Fig. 1.

The pulse generator (Berkeley Nucleonics Corporation (BNC 565)) delivers 70 ns impulsions with a 1% duty cycle that are used in conjunction with a temperature or a subthreshold current ramp in order to obtain the laser wavelength variation. When using a temperature ramp, the laser temperature is scanned step by step, with typically 100 ms between successive steps. The series of impulsions are sent (using the driver from Alpes Laser starter kit which in part composed by a DEI PCO-7120 card) to the QC laser placed inside a Laser Laboratory Housing from Alpes Lasers. The laser beam passes through the absorption path cell containing ammonia ($L = 20$ cm) and is collected by SAT1903N high-speed MCT detector. The detector's signal is then sent to a digital sampling oscilloscope (Lecroy Waverunner104 Xi) so that each optical pulse is recorded. A part of the laser beam is sent through a Germanium etalon (with a FSR of 0.048 cm^{-1}) to a Kolmar detector in order to obtain the wavenumber calibration. Absorption features can be seen either inside each pulse (i.e. versus time) or at a constant delay inside successive pulses, versus subthreshold ramp/substrate temperature.

Each of spectra presented in this paper have been built using the intermediate-size method described in our previous paper [14]. Each pulse is recorded by the digital oscilloscope and a post-treatment permits one to rebuild the spectrum by selecting a constant delay inside pulses. The baseline due to the power variation of the laser during the

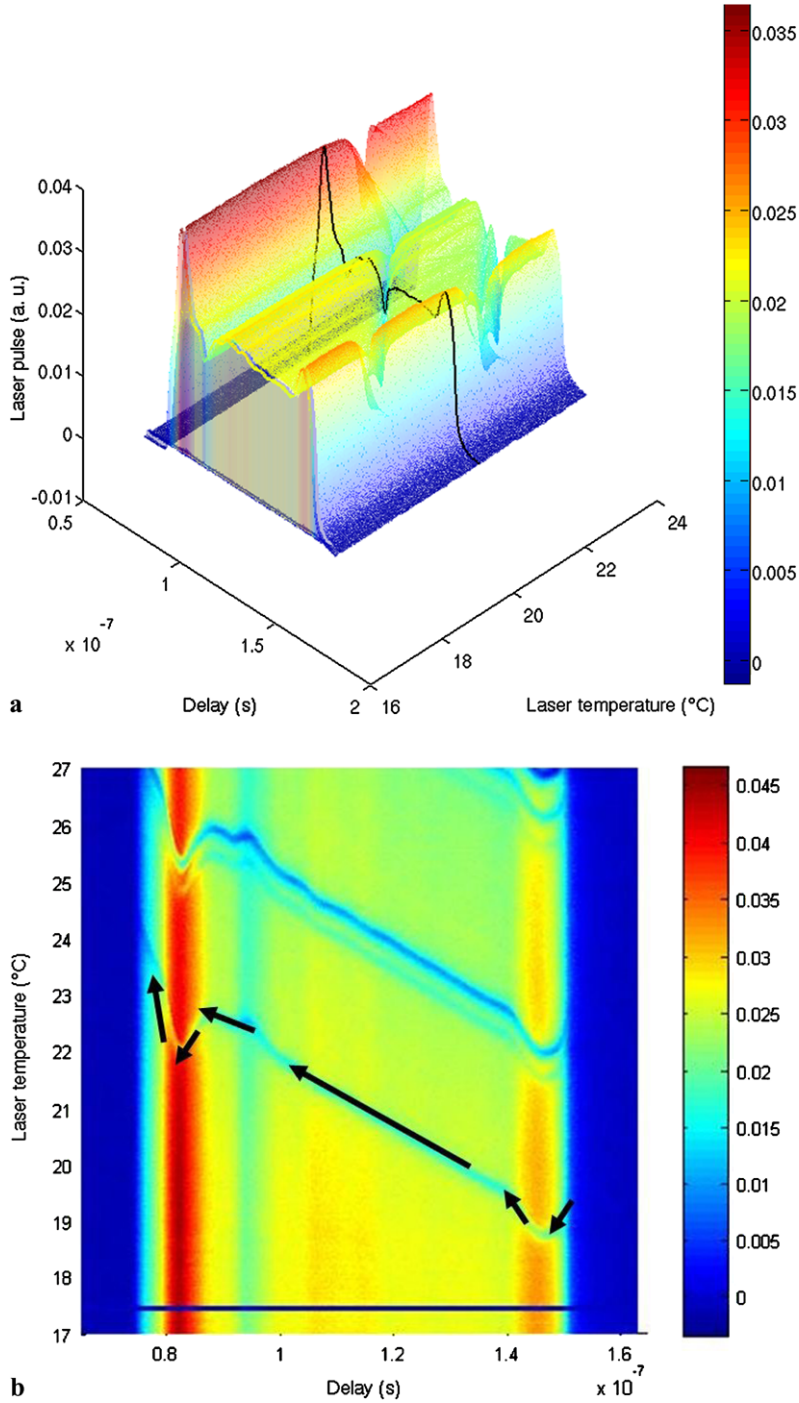

Fig. 2 (**a**) 3D view of successive experimental laser pulses (NH_3/air spectrum, $P = 60$ mbar, Concentration # 0.3%, Temperature # 296 K, Length = 20 cm). Successive laser pulses are presented versus the laser substrate temperature. The black trace corresponds to one pulse. (**b**) Top view of Fig. 2(a)

ramp is also taken into account during this post-treatment operation. Figure 2 presents the experimental data corresponding to 3000 successive measurements recorded during a substrate temperature ramp ranging from 17 to 27°C. Each measurement is in fact the average of 10 successive pulses and corresponds to one step of the temperature scanning. The total time for one measurement of about 7 µs is negligible when compared to the duration of one temperature step. Figure 2(a) is a 3D representation of the 3000 measurements made between 17 and 27°C. The signal amplitude (measured optical power) is coded using the color scale given on the right of the figure, from blue (no signal) to red (maximum of signal). The pulse recorded at $T = 21$°C is plotted in black. Figure 2(b) corresponds to a top view of Fig. 2(a). Each measurement corresponds to one horizontal line on Fig. 2(b). The horizontal scale represents the pulse length and the vertical scale gives the substrate temperature corresponding to each measurements. According to the

color coding, the maximum of absorption appear as the thin blue lines.

Figure 2(b) can be used to follow the moving of the absorption line inside the pulse during the substrate temperature ramp. This is materialized by the arrows on the Fig. 2(b). This moving is an important clue to understand the variation of the instantaneous wavenumber versus the substrate temperature. In the middle of the pulse (typically between 1 and 1.4×10^{-7} s on Fig. 2(b)), the emitted wavenumber varies in a very regular manner: the frequency downchirp can be exactly compensated by a substrate temperature variation and the absorption line shifts nearly linearly. In both transients at the beginning and at the end of the pulse, the emitted wavenumber varies very differently at a given substrate temperature the same absorption feature can be seen twice in one pulse (see for example between 22 and 23°C and for a time delay about 0.8×10^{-7} s). The arrows allow us to follow the value of the instantaneous chirp frequency, which is directly linked to the variation in heating during the pulse. One can see that the sense of this one change rapidly and is also more important in transients than in the rest of the pulse.

Figure 2 also allows us to compare the spectral range due to frequency downchirp and to the substrate temperature variation: at a given temperature (21°C for example) only one absorption feature (at 967.997761 cm^{-1}) can be seen inside a pulse. The substrate temperature variation (for example for a delay inside the pulse of 1.2×10^{-7} s) allows one to scan several absorption features (one line at 967.997761 cm^{-1} and a doublet at 967.774745 and 967.738421 cm^{-1}). The first alternative can be used for narrow and isolated spectral lines (i.e. at low pressure) whereas the second alternative should be preferred at higher pressures. Results on NH_3 in the 10 µm region will be presented in this paper: in the low-pressure range (1 mbar range—Sect. 2) and in the mid-pressure range (50 mbar range—Sect. 3).

2 Low-pressure (mbar range) spectra of ammonia

An example of recorded pulse of ammonia at low pressure with the intermediate-size pulse technique and without added ramp is presented in Fig. 3. Figure 3(a) features a 70 ns pulse at a laser temperature without absorption and Fig. 3(b) features a recorded pulse at a laser temperature where ammonia absorbs. In both cases the first part of the pulse presents a transient and is followed by a regular frequency downchirp area. The last part of the pulse also presents a transient. The Fabry–Pérot etalon transmission shown on Fig. 3(b) allows us to determine the frequency downchirp tuning rate in this useful part of the pulse. At these low pressures the spectrum due to the chirp of the laser into the pulse let oscillations appears after the absorption. This phenomenon is named the rapid-passage effect and was observed with the intrapulse technique in [17].

The oscillations observed during the pulse cannot be explained by the Beer–Lambert law. The lifetimes of the levels that are linked to the Einstein coefficients and that are the basics of this law cannot take into account the individual comportment of the atoms. In this case there is no more equilibrium in the interaction between radiation and matter. A more realistic representation can be obtained thanks to a semi-classical model as was initially proposed by Duxbury team [17, 18, 20]. In this model the electromagnetic field is represented in a classical manner via the Maxwell equations and the atomic part is described by quantum mechanics.

This description is known as the Maxwell–Bloch equations. The Bloch differential equations are obtained by combining the coherent effect of the wave with the effect of a random phenomenon such as spontaneous emission and collisions. These equations can be presented by the following system [21]:

$$\frac{d\bar{u}}{dt} = -\frac{1}{\tau_2}\bar{u} + \delta\omega\bar{v}, \tag{1}$$

$$\frac{d\bar{v}}{dt} = -\delta\omega\bar{u} - \frac{1}{\tau_2}\bar{v} - \Omega_1\bar{m}, \tag{2}$$

$$\frac{d\bar{m}}{dt} = \Omega_1\bar{v} + \frac{m_0 - \bar{m}}{\tau_1}. \tag{3}$$

In this system $\bar{u}$ and $\bar{v}$ represent the mean values of the two crossed variables of the Bloch system. They are linked to the electric dipolar moment because the stationary solutions of this system permit to determine the dielectric susceptibility of the medium. $\bar{m}$ corresponds to the inversion of population and m_0 represents the initial value of the inversion of population. $\delta\omega$ represents the difference between the pulsation of the incident wave and the central pulsation of the transition and is related to the frequency downchirp tuning rate. τ_1 and τ_2 are linked to the lifetime of the levels. Finally Ω_1 represents the Rabi pulsation.

Analytical solutions of this system can be found when $\delta\omega$ remains constant during the experiment. Due to frequency downchirp $\delta\omega$ varies during each pulse and only numerical resolution of this system can be done. One important difference between the analytical solutions and the numerical solutions is that the oscillations in $\bar{u}$, $\bar{v}$ and $\bar{m}$ do not have a constant frequency. Moreover, as was demonstrated in [20], the resolution of this system do not allow to reproduce the observed signals and several effects must be included in the calculation:

- The velocity of the molecules affects the value of $\delta\omega$ due to Doppler effect. The system of coupled equation must be solved for several classes of velocities (200).

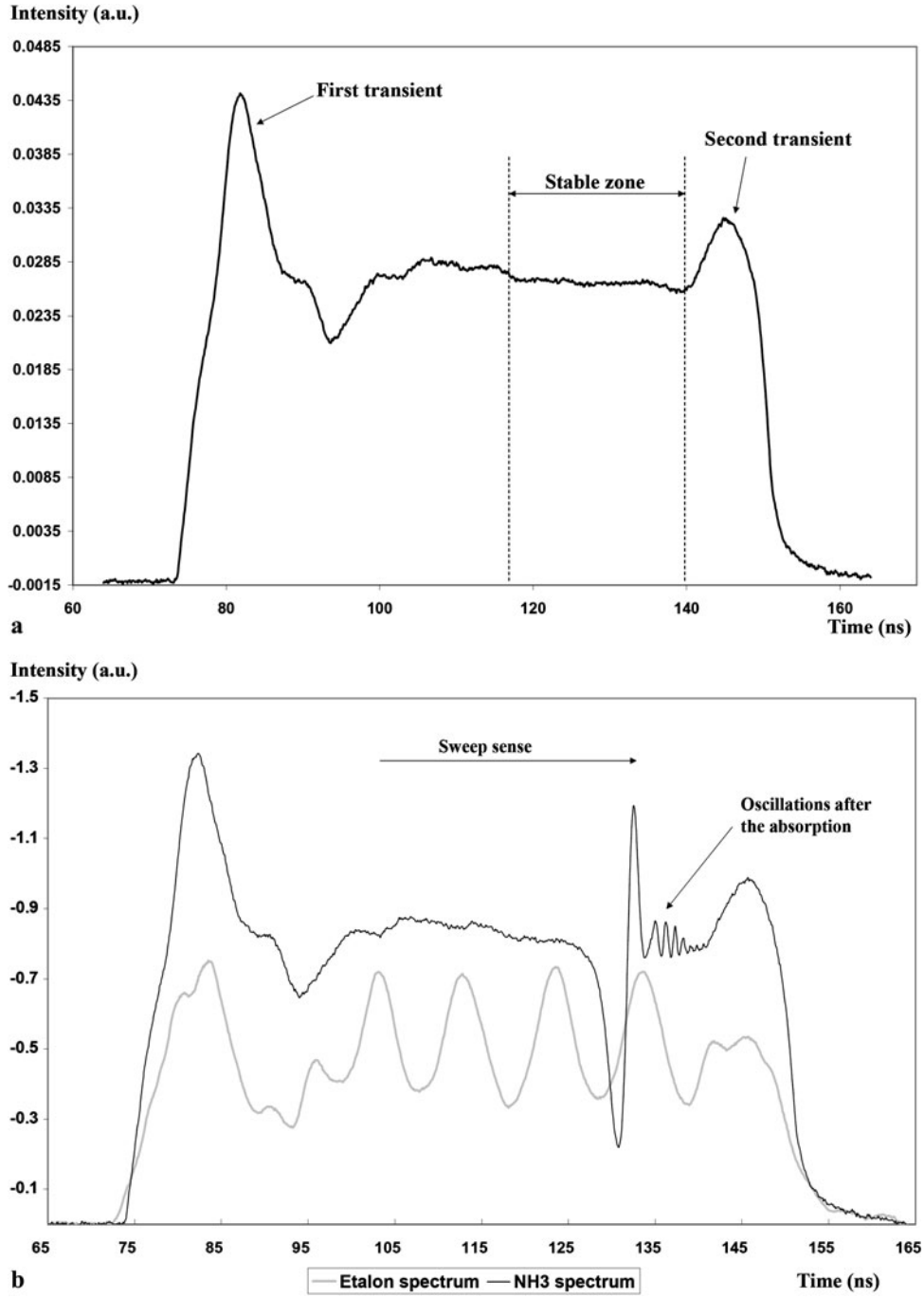

Fig. 3 (**a**) Record of a pulse with the intermediate-size pulse technique and (**b**) observation of rapid-passage effect in a 70 ns pulse with 0.37 mbar of pure ammonia

- The Rabi pulsation used in (2) and (3) is related to the transition dipole moment. The arbitrary orientation of the molecule versus the laser field must also be included in the calculation.

These two effects smooth the very fast oscillations observed in the solutions of (1), (2) and (3) and allow us to obtain a satisfactory agreement with observed signals. Some examples are presented on Fig. 4. Figure 4(a) presents some recorded signals at several pressures and Fig. 4(b) presents the results of the calculations. At this moment we do not obtain full agreement between measurements and calculations. As only numerical solutions can be obtained, they cannot be used in a typical inversion process like least-squares fitting. However, the overall agreement on the three pressure range is good.

The best solution to obtain spectra that are satisfactory from a spectroscopic point of view is to increase the pressure. In this case the lifetime τ_1 becomes very small and the second term of (3) $\frac{m_0-\bar{m}}{\tau_1}$ becomes larger than the first one $\Omega_1\bar{v}$; thus the oscillations disappear. Section 3 of this pa-

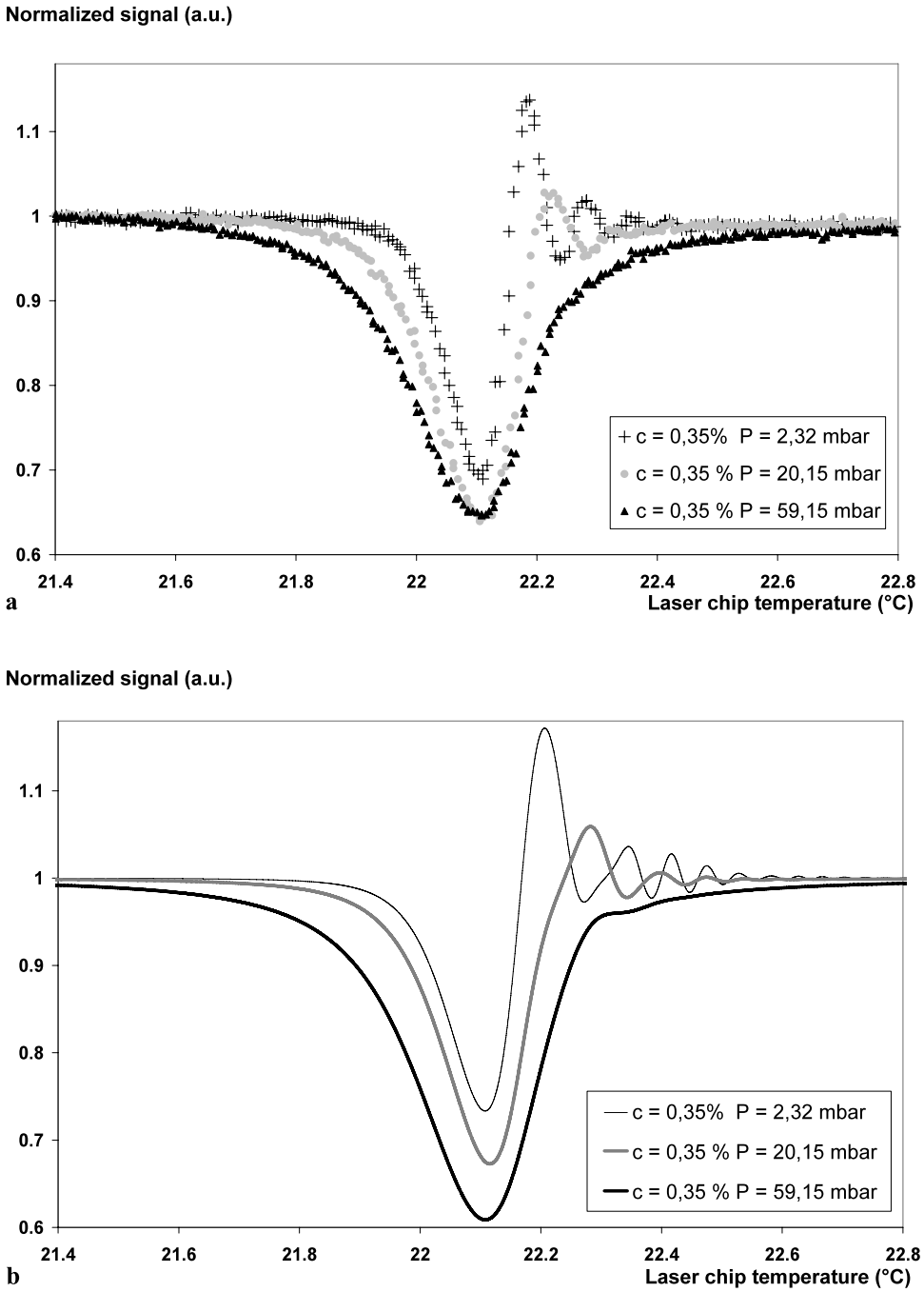

Fig. 4 (**a**) Recorded signals for different gas pressures. (**b**) Calculated signals for the same experimental conditions

per will present results obtained at higher pressures where rapid-passage effects do not exist anymore.

3 Mid-pressure (50 mbar range) spectra of ammonia

In this part either temperature or current ramps were added to the 70 ns length duration pulses. A spectrum corresponding to a 40 ns delay after the beginning of the pulse is presented in Fig. 5. This spectrum is very satisfactory from a spectroscopic point of view and can be directly compared to a calculation using Voigt profile and HITRAN parameters [22]. The fitted and experimental spectra are very similar. Numerous spectra were recorded at different pressures from 50 to 80 mbar. For all those spectra the collisional line width was fitted and compared to the HITRAN value. The fitting procedure has been described in detail in [23]. The experimental and HITRAN collisional line widths are plotted vs. pressure in Fig. 6. One can remark than the two lines are parallel; however, only the HITRAN curve passes through zero. This is the demonstration of the existence of an apparatus function.

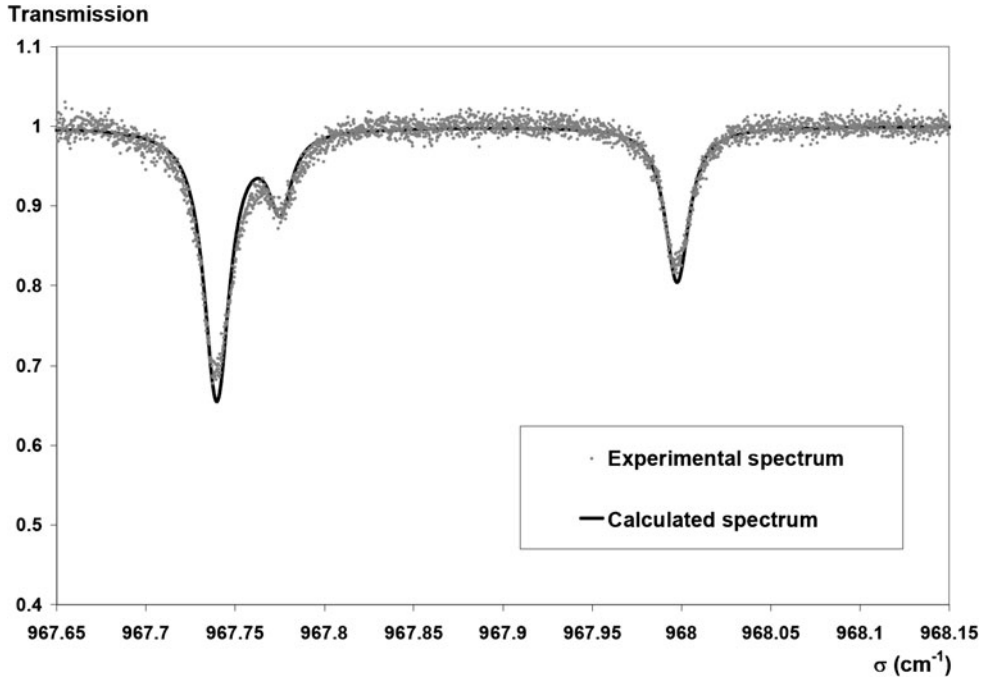

Fig. 5 Example of spectrum recorded with a temperature ramp of 10 K and comparison with a calculated spectrum using Voigt profile for a pressure = 71 mbar and concentration of NH_3 in air is 1.3%

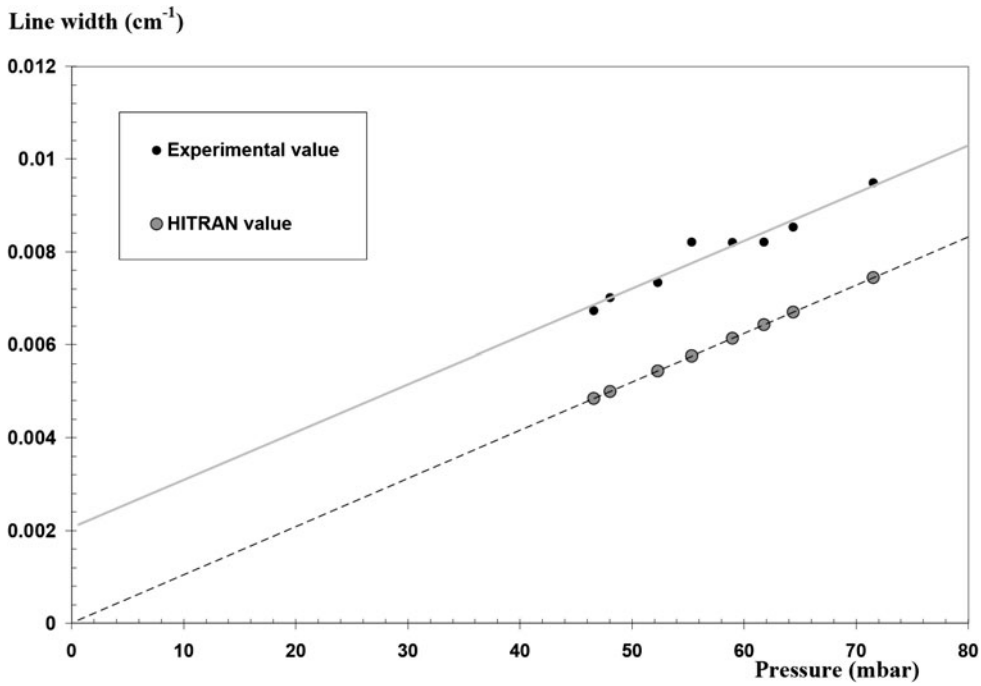

Fig. 6 Fitted line width vs. pressure for the experimental spectra. The HITRAN values are also displayed. See text for more details

The existence of an apparatus function is also demonstrated in Fig. 7. Figure 7(a) features the NH_3 absorption line using a temperature ramp and the comparison with the calculated spectrum using HITRAN data. Figure 7(b) shows the same line recording using a subthreshold current ramp. Note that the difference between the two techniques is that the temperature spectrum is longer to record (typ. 140 s) than the current one (typ. 10 ms). On the other side the current spectrum is less wide than the temperature one. For these pressures there is no problem but it may be a drawback for atmospheric pressure spectra.

Even if the experimental and HITRAN calculated spectra are similar, some differences remain. To confirm that these differences were due to the apparatus function, we calculate the HITRAN spectrum using Voigt profile and convoluted it by a Gaussian profile with $\Delta\nu = 0.003$ cm^{-1}. These calculations are also displayed in Figs. 7(a) and 7(b). For these two figures one can clearly see that the experi-

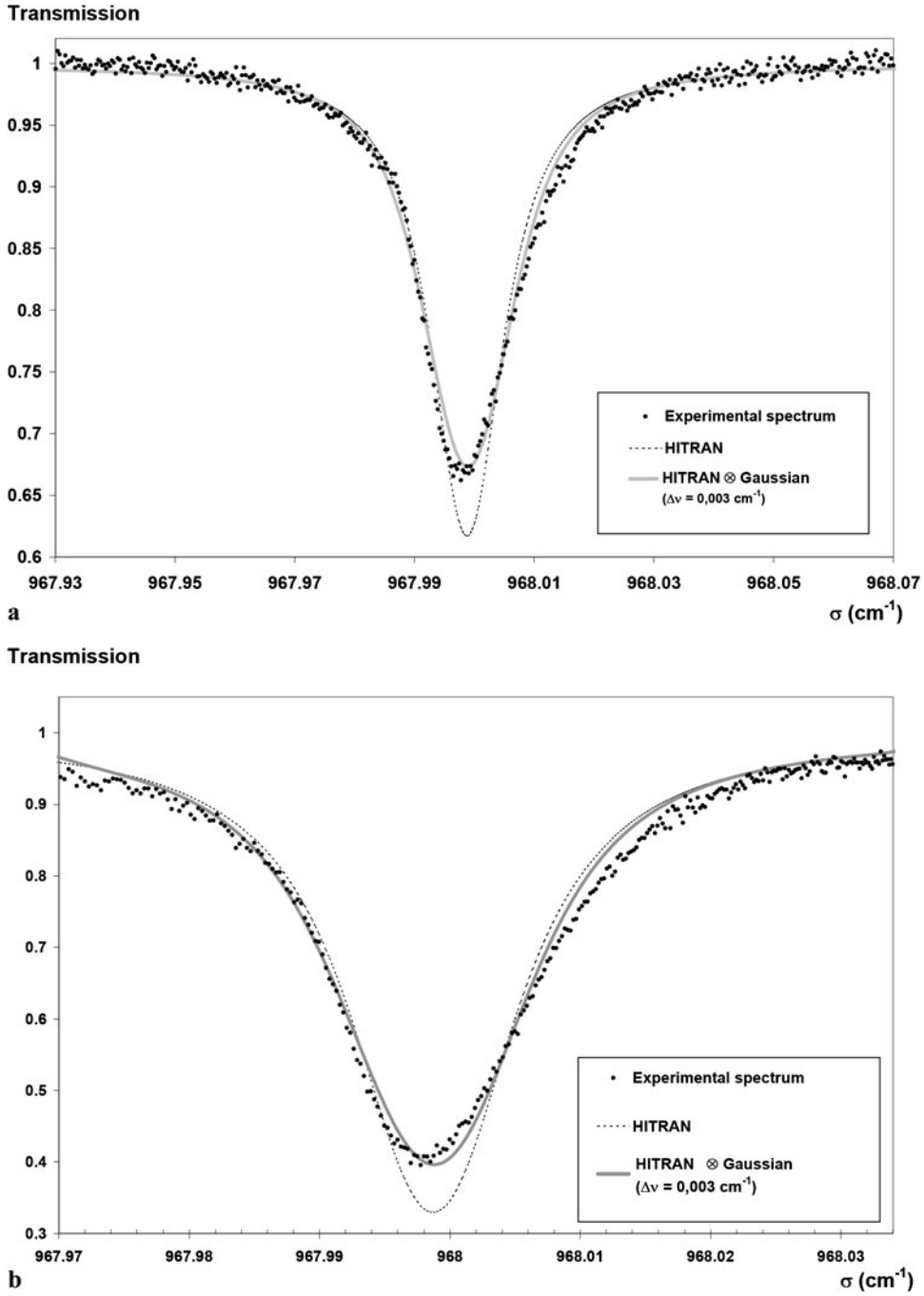

Fig. 7 Transmission experimental spectra with (**a**) a temperature ramp ($P = 58$ mbar and 0.28% of NH_3 in air) and (**b**) a current ramp ($P = 51$ mbar and 0.8% of NH_3 in air). On both parts of the figure are also displayed the calculated spectra using Voigt profile with the HITRAN data and another calculation introducing a convolution of the HITRAN spectra with a Gaussian lineshape (see text for more details)

mental spectra and the new calculation are very well fitted. The small difference remaining in the two spectra (on the right part of the wing) is probably due to a remaining part of the rapid-passage effect. The recorded and calculated spectra allows estimating the effective line width of the laser to be about 0.003 cm^{-1}, which is significantly shorter than typical values reported with shorter pulses (typically 0.015 cm^{-1} [12]). Thus the intermediate-size pulse technique is more satisfactory from a spectroscopic point of view.

4 Conclusion

Pulsed quantum-cascade-laser spectrometers are still used to detect atmospheric gases. We have previously demonstrated [14] that neither the interpulse nor the intrapulse technique was totally satisfactory to use the pulsed QCLs. The interpulse (short-pulse) technique gives distorted spectra and the intrapulse (long-pulse) technique cannot be applied to all QCLs. Thus we have developed the intermediate-size pulse technique for gas detection using pulsed QCL spectrome-

ters. This technique was applied in this paper to record infrared spectra of ammonia in the 10 µm region. However, NH_3 spectra recorded in the mbar range show typical oscillations after the absorption due to the rapid-passage effect. This phenomenon had been previously observed with the intrapulse technique [17]. In this paper, the resolution of the Maxwell–Bloch equations has demonstrated a good agreement in comparison with experimental results at various pressures.

To realize correct spectroscopic measurements NH_3 spectra were recorded in the 50 mbar range, where the oscillations disappear. Thus the intermediate-size pulse technique gives reliable measurements for NH_3 detection using a temperature or a current ramp. Moreover, the typical apparatus function (0.003 cm^{-1} HWHM) is far lower from the typical apparatus function of the interpulse QCL spectrometers (0.015 cm^{-1} HWHM).

Acknowledgements The authors are indebted to the *Région Champagne-Ardenne* for financially supporting of the PhD of Bruno Grouiez.

References

1. L. Joly, V. Zéninari, B. Parvitte, D. Weidmann, D. Courtois, Y. Bonetti, T. Aellen, M. Beck, J. Faist, D. Hofstetter, Appl. Phys. B, Lasers Opt. **77**, 703 (2003)
2. B. Parvitte, L. Joly, V. Zéninari, D. Courtois, Spectrochim. Acta A **60**, 3285 (2004)
3. L. Joly, V. Zéninari, B. Parvitte, D. Courtois, G. Durry, Opt. Lett. **31**, 143 (2006)
4. A. Grossel, V. Zéninari, L. Joly, B. Parvitte, G. Durry, D. Courtois, Spectrochim. Acta A **63**, 1021 (2006)
5. A. Grossel, V. Zéninari, B. Parvitte, L. Joly, G. Durry, D. Courtois, Infrared Phys. Technol. **51**, 95 (2007)
6. A. Grossel, V. Zéninari, B. Parvitte, L. Joly, D. Courtois, Appl. Phys. B, Lasers Opt. **88**(3), 483 (2007)
7. L. Joly, C. Robert, B. Parvitte, V. Catoire, G. Durry, G. Richard, B. Nicoullaud, V. Zéninari, Appl. Opt. **47**, 1206 (2008)
8. A. Grossel, V. Zéninari, B. Parvitte, L. Joly, G. Durry, D. Courtois, J. Quant. Spectrosc. Radiat. Transfer **109**, 1845 (2008)
9. B. Grouiez, B. Parvitte, L. Joly, D. Courtois, V. Zéninari, Appl. Phys. B, Lasers Opt. **90**, 177 (2008)
10. J. Faist, F. Capasso, D.L. Sivco, C. Sirtori, A.L. Hutchinson, A.Y. Cho, Science **264**, 553 (1994)
11. J. Devenson, O. Cathabard, R. Teissier, A.N. Baranov, Appl. Phys. Lett. **91**, 141106 (2007)
12. K. Namjou, S. Cai, E.A. Whittaker, J. Faist, C. Gmachl, F. Capasso, D.L. Sivco, A.Y. Cho, Opt. Lett. **23**, 219 (1998)
13. A.A. Kosterev, F.K. Tittel, C. Gmachl, F. Capasso, D.L. Sivco, J.N. Baillargeon, A.L. Hutchinson, A.Y. Cho, Appl. Opt. **39**, 6866 (2000)
14. B. Grouiez, B. Parvitte, L. Joly, V. Zéninari, Opt. Lett. **34**, 181 (2009)
15. E. Normand, G. Duxbury, N. Langford, Opt. Commun. **197**, 115 (2001)
16. E. Normand, M. McCulloch, G. Duxbury, N. Langford, Opt. Lett. **28**, 16 (2003)
17. M. McCulloch, G. Duxbury, N. Langford, Mol. Phys. **104**, 2767 (2006)
18. M.T. McCulloch, E.L. Normand, N. Langford, G. Duxbury, D.A. Newnham, J. Opt. Soc. Am. B **20**, 1761 (2003)
19. www.alpeslasers.ch
20. G. Duxbury, N. Langford, M.T. McCulloch, S. Wright, Mol. Phys. **105**, 741 (2007)
21. L. Allen, J.H. Eberly, *Optical Resonance and Two-Level Atoms* (Dover, New York, 1975)
22. L.S. Rothman, D. Jacquemart, A. Barbe, D. Chris Benner, M. Birk, L.R. Brown, M.R. Carleer, C. Chackerian Jr., K. Chance, L.H. Coudert, V. Dana, V.M. Devi, J.-M. Flaud, R.R. Gamache, A. Goldman, J.-M. Hartmann, K.W. Jucks, A.G. Maki, J.-Y. Mandin, S.T. Massie, J. Orphal, A. Perrin, C.P. Rinsland, M.A.H. Smith, J. Tennyson, R.N. Tolchenov, R.A. Toth, J. Vander Auwera, P. Varanasi, G. Wagner, J. Quant. Spectrosc. Radiat. Transfer **96**, 139 (2005)
23. V. Zéninari, B. Parvitte, L. Joly, T. Le Barbu, N. Amarouche, G. Durry, Appl. Phys. B, Lasers Opt. **85**, 265 (2006)